Solar Phys
DOI 10.1007/s11207-011-9763-0

Correlation Analyses Between the Characteristic Times of Gradual Solar Energetic Particle Events and the Properties of Associated Coronal Mass Ejections

Z.H. Pan · C.B. Wang · Yuming Wang · X.H. Xue

Received: 1 December 2010 / Accepted: 28 March 2011

Abstract It is generally believed that gradual solar energetic particles (SEPs) are accelerated by shocks associated with coronal mass ejections (CMEs). Using an ice-cream cone model, the radial speed and angular width of 95 CMEs associated with SEP events during 1998 – 2002 are calculated from SOHO/LASCO observations. Then, we investigate the relationships between the kinematic properties of these CMEs and the characteristic times of the intensity-time profile of their accompanied SEP events observed at 1 AU. These characteristic times of SEP are *i*) the onset time from the accompanying CME eruption at the Sun to the SEP arrival at 1 AU, *ii*) the rise time from the SEP onset to the time when the SEP intensity is one-half of peak intensity, and *iii*) the duration over which the SEP intensity is within a factor of two of the peak intensity. It is found that the onset time has neither significant correlation with the radial speed nor with the angular width of the accompanying CME. For events that are poorly connected to the Earth, the SEP rise time and duration have no significant correlation with the radial speed and angular width of the associated CMEs. However, for events that are magnetically well connected to the Earth, the SEP rise time and duration have significantly positive correlations with the radial speed and angular width of the associated CMEs. This indicates that a CME event with wider angular width and higher speed may more easily drive a strong and wide shock near to the Earth-connected interplanetary magnetic field lines, may trap and accelerate particles for a longer time, and may lead to longer rise time and duration of the ensuing SEP event.

Keywords Characteristic times · CME · Ice-cream cone model · SEP events

1. Introduction

According to the definition of the International Space Environment Service, a solar energetic particle (SEP) event occurs when the peak intensity of the integrated flux of energetic pro-

Z.H. Pan · C.B. Wang (✉) · Y. Wang · X.H. Xue
CAS Key Laboratory of Basic Plasma Physics, School of Earth and Space Sciences,
University of Science and Technology of China, Anhui 230026, China
e-mail: cbwang@ustc.edu.cn

Published online: 11 May 2011

tons greater than 10 MeV is above the threshold of 10 pfu ($cm^{-2}\ s^{-1}\ ster^{-1}$). SEP events, following Reames (1999) and Kallenrode (2003), can be classified as impulsive type and gradual type. Impulsive SEP events are generally considered to be the result of solar flares, when particles are accelerated during the rapid release of magnetic energy via a magnetic reconnection mechanism. Gradual SEPs are continually accelerated by shock waves driven out of the corona by a fast coronal mass ejection (CME). As a result, gradual SEP events normally have longer duration and stronger intensity than impulsive SEPs. Although there are still arguments (Kocharov *et al.*, 1999; Kahler, McAllister, and Cane, 2000; Torsti *et al.*, 2001; Tang and Dai, 2003; Tylka *et al.*, 2005; Dai, Tang, and Qiu, 2005) about whether the excitation of gradual SEP events involves any phases of solar flares, CME-driven shocks are assumed to be the sole source of gradual SEP events in this paper.

Assuming that gradual SEPs are accelerated by CME-driven shocks, one may expect to find a close relationship between the characteristics of a gradual SEP intensity-time profile and the properties of the associated CMEs. The possible formation and ensuing intensity of a SEP event may significantly depend on the strength of the associated CME-driven shock and the multiple acceleration processes in which particles can be entrapped by the shock front (Reames, 1999; Tylka, 2001; Kallenrode, 2003). A faster CME would likely drive a stronger shock. Reames, Kahler, and Ng (1997) figured out that a SEP event always appears when a shock speed is greater than 750 $km\ s^{-1}$, and is likely to appear for a shock speed of 500 – 750 $km\ s^{-1}$. By statistically analyzing the correlation between the intensity-time profiles of SEP events at 1 AU and the characteristic parameters of CME events near the Sun, Kahler (2005) found the results consistent with the interpretation that a faster CME could drive a stronger shock with a longer duration, and that the time for particle acceleration across the shock front is correspondingly increased.

The CME width can also affect the characteristic times of gradual SEP events significantly. During the anti-Sunward propagation of a CME-driven shock, the junction point of the interplanetary magnetic field (IMF) connected to the Earth is shifted from west to east. If the width of a CME is larger, the CME-driven shock would also have a wider extent. As a result, the time necessary for the Earth-connected IMF lines to cross the shock front is longer, the capture and acceleration of particles along these IMF lines could last much longer, and the duration of the SEP event is extended. Meanwhile, conditions for the particle acceleration are significantly different for a quasi-parallel shock and a quasi-perpendicular shock (Jokipii, 1982; Kahler, 2001; Tylka and Lee, 2006). Jokipii (1987) concluded that the initial particle speed for acceleration at a quasi-perpendicular shock must be much higher than the shock speed, whereas injection at a quasi-parallel shock can occur when the initial particle speed is only slightly larger than that of the shock. Acceleration time scales at quasi-parallel shocks can be orders of magnitude longer than those of quasi-perpendicular shocks (Jokipii 1982, 1987; Decker and Vlahos, 1986; Ostrowski, 1991; Webb *et al.*, 1995; Giacalone 2005a, 2005b). Although *in situ* properties of CME-driven shocks cannot be observed along a complete shock front, it is expected that a wider CME could more easily drive a quasi-parallel shock at the Earth-connected IMF lines, and lead to more particles being accelerated for a longer time (Kahler, 2004). The correlation of a SEP event intensity with the angular width of CMEs may be greater than previously thought, whereas its correspondence to the ambient solar wind is insignificant, as proposed by Kahler and Reames (2003) on the basis of evidence that no gradual SEP events are associated with CMEs faster than 900 $km\ s^{-1}$ and narrower than 60°. Gopalswamy *et al.* (2001) found that CMEs associated with type II radio bursts in decameter-hectometer wavelengths, a strong signature (Cliver, Kahler, and Reames, 2004) of SEP events, were significantly wider (102° versus 66°) than the fast ($> 900\ km\ s^{-1}$) CMEs without those radio bursts. Kahler and Vourlidas (2005) classified fast and wide CMEs during 1998 – 2002, erupted from the western side

of solar disk, into two groups according to the large and small intensities of their associated SEP events, and then found that a larger angular width and greater plasma density are more favorable for the occurrence of SEP events. Furthermore, Kahler (2005) found that there is a weak correlation between the projected angular width of CMEs and the characteristic times of SEP events.

The preceding studies on the correlation between the characteristic times of SEP events and the properties (namely, the speed and angular width) of CME events are generally based on the projected values of CMEs on the plane of the sky. However, large differences may exist between true parameter values of a CME and its projection onto the plane of the sky, particularly for halo and partial-halo CMEs. For instance, a halo CME with a true angular width of 60° could be projected to show a width of 360° within the plane of the sky. However, by using some geometrical models of CMEs such as the cone model, the true radial speed and angular width of CMEs, particularly for halo CMEs, can be inferred from the plane-of-the-sky measurements by SOHO/LASCO (Howard *et al.*, 1982; Fisher and Munro, 1984; Leblanc *et al.*, 2001; Zhao, Plunkett, and Liu, 2002; Michalek and Gopalswamy, 2003; Xie *et al.*, 2006; Xue, Wang, and Dou, 2005). The previous studies on the characteristic times of SEP events and their dependences on the associated CME properties could be substantially improved by adopting the cone-model properties, instead of the projection values, of CMEs, as suggested by Kahler (2005). In this paper, an ice-cream cone model is used to estimate the kinematic parameters of 95 CME-associated SEP events during 1998 – 2002, namely, their radial speeds, angular widths, and source regions. Then, the relationships between the characteristic times of SEP intensity-time profiles observed at 1 AU and the kinematic parameters of associated CMEs are reanalyzed.

2. Observation Data and Analysis Method

2.1. Cone Model of CMEs

The morphology of CMEs can be approximated as a cone or an elliptical cone (Howard *et al.*, 1982), as limb CMEs observed by SOHO/LASCO have a nearly constant angular width during its anti-Sunward propagation. With the assumption of invariant angular width of an out-moving CME, true radial speed and angular width can be derived from the projected image on the plane of the sky. Recently, several cone or ice-cream cone models of CMEs have been proposed (Fisher and Munro, 1984; Leblanc *et al.*, 2001; Zhao, Plunkett, and Liu, 2002; Michalek, Gopalswamy, and Yashiro, 2007 (MGY); Xie, Ofman, and Lawrence, 2004; Xue, Wang, and Dou, 2005).

Interestingly, the kinematic parameters determined by the cone models are better approximations of the true spatial parameters of CMEs. For example, Michalek *et al.* (2004) calculated the Sun–Earth transit times of 49 front-side halo CMEs in the period 1996 – 2002. Instead of directly using the projected speed in the sky plane, the radial speed of a CME was first inferred from the MGY cone model, and then inputted to the empirical shock arrival (ESA) model (Gopalswamy *et al.* 2005a, 2005b). The absolute error of the transit time between the model and the observation is reduced from 11.2 h to 8.7 h. Following the same methodology, Michalek, Gopalswamy, and Yashiro (2007) found a significant correlation between the Sun-Earth transit time of CMEs and the geomagnetic storm index *Dst*. This correlation would degrade to one half, if the projected speed of CMEs were directly used. Similarly, applying three cone models to 40 Earth-directed halo CMEs observed in 1998 – 2003, and inputting the derived radial speed of CMEs to the ESA model to obtain

the Sun-Earth transit time, Xie, Ofman, and Lawrence (2004) found that the prediction accuracy is improved by 46% compared to the case of direct usage of CME projected speed. Moreover, Wang *et al.* (2006), by combining the ice-cream cone model (Xue, Wang, and Dou, 2005) in the corona and the kinematic model (Wang *et al.*, 2004) in the interplanetary space, calculated the angular width and possible deflected trajectory of CMEs and found a match between the models and observations. All of these examples show that it is reliable to infer the geometrical parameters of CMEs from the cone models.

In this paper, the ice-cream cone model proposed by Xue, Wang, and Dou (2005) is adopted to reconstruct the kinematic properties of CMEs. This ice-cream cone model, which is based on a least-squares fitting of the projected CME speed along different polar angles within the plane of the sky, can be applied to either halo or non-halo CMEs. Three main steps are used to calculate the radial speed, angular width, and source location of a CME: *i*) restricting its possible source region on the solar surface by using images from the SOHO/ EUV Imaging Telescope (EIT) or occasionally from the *Yohkoh* Soft X-ray Telescope (SXT); *ii*) measuring its projected speeds along different polar angles from the difference images of LASCO/C2 and LASCO/C3; *iii*) in the possible source region estimated in step 1, using a least-squares fitting method to obtain the optimal parameters.

2.2. Selection of SEP Events

In our study, 95 gradual SEP events accompanied by CME events are identified from observation data between 1998 and 2002. The selection and characteristic times of SEP events refer to the data summarized by Kahler (2005). Because the exact heliographic location of the solar source region is not now available for back-side CMEs, only front-side CMEs are selected for the association with SEP events. The observation data and model results for the selected CMEs are summarized in Table 1; the first column is the observation date. The initiation time, radial speed, angular width, and source region of CMEs estimated using the ice-cream cone model are listed in columns 2, 3, 4, and 8, respectively. The height-time profile of the initial phase of a CME is deduced by the extrapolation of radial speed fitted with the ice-cream cone model, and then the departure time of the leading edge of the CME from the solar disk is considered as the initial time of the CME eruption.

A few events are ruled out from our statistical studies, in which blurred observation images or complex CME structures may lead to unreliable measurements of projected geometry. Also, in some cases, the leading edges of CMEs are quite irregular. For these irregular CMEs, the projected geometry is obviously asymmetric, or the speed at the central part is much greater than that at the flank part. If these CMEs are non-halo (width $< 180°$) and their source regions are near the solar limb, the projected parameters, which should be close to the true geometry parameters, are directly used as a reasonable approximation to their true values. These events are denoted as b and c in Table 1. However, if the irregular CMEs are halo or their source regions are near the center of the solar disk, the projected parameters deviate largely from the true parameter values, and such CME cases are ignored in the analyses of this paper.

2.3. Characteristic Times of SEP Events

The characteristic times of SEP events in this paper are the same as those defined by Kahler (2005). For every SEP event, three characteristic times, T_{O}, T_{R}, and T_{D}, are identified. T_{O} refers to the interval between the initiation time of CME eruption on the Sun and the arrival time of the SEP event at 1 AU. T_{R} is the rise time of the SEP event, defined as the interval

Table 1 Parameter list of SEP events and their associated CME events in 1998 – 2002[a].

CME date	Initial T (UT)	V (km s^{-1})	W (°)	T_O (h)	T_R (h)	T_D (h)	Source region
1998							
980420 [b]	9:55	1863	165	1.6	12.5	36	S43W90
980502	13:25	799	108	1.1	2	8.5	N10W20
981105	18:17	910	66	3.7	11	6	N11W14
1999							
990503	5:49	1289	109	12.7	11.5	33	N19E34
990509	16:15	428	91	2.3	1	4.5	N20W80
990604	5:48	1771	66	2.7	1.5	18	N13W26
990627	8:11	725	118	3.4	2	9	N30W30
990629	6:46	592	145	5.2	27	37	N20E02
990828	17:58	572	131	3	1	12.5	S15W16
991014	8:45	1320	76	10.3	9	46	N11E16
2000							
000118	17:20	674	116	2.6	2	42	S10E20
000217	21:08	613	139	0.9	2	...	S20W06
000302	8:05	776	62	1.9	2	8	S14W52
000303	1:31	777	60	2	0.5	3	S24W69
000404	15:08	1094	122	1.4	5.5	15.5	N12W39
000427	14:27	982	40	2.1	0.5	10	N21W80
000504[b]	10:53	1404	170	1.1	4	22	S17W90
000505	15:18	1566	110	4.7	10	32	S08W34
000515	15:49	1074	102	3.6	2.5	8.5	S12W50
000602	21:09	736	105	9.4	11	30.5	N16E66
000606	15:20	1074	163	4.2	21.5	16	N06E30
000610	15:25	1002	104	1	0.5	7	N11W17
000615[b]	19:25	1081	116	1.6	1	15.5	N29W65
000617	2:50	838	97	3	0.5	7.5	N17W64
000618	2:04	654	104	0.4	1	6.5	N29W71
000623	14:25	818	114	0.7	1.5	3.5	N26W61
000625	7:42	1617	165	3.8	2.5	17.5	N16W55
000628	18:45	1156	135	1.8	1	8.5	N12W71
000710	21:19	1125	95	1.2	4.5	10.5	N16E35
000711	12:39	1033	117	2.4	1	32	N08E20
000714	10:04	1576	89	1.5	1.5	26	N02W09
000722	11:21	1043	54	1.2	1	9.5	N08W46
000812	13:56	900	57	2.1	1	12	N20W35
000909	8:02	592	69	2.9	1	9	N12W55
000912	11:45	1555	101	1.7	5.5	26	S12W20
000919	8:10	766	76	4.8	2	18	N14W46
001009	22: 28	581	115	8.5	7	43	N20W10
001025	9:12	900	97	3.3	5	16.5	N01W20
001108	22:48	1729	144	0.7	3.5	15	N10W50

Table 1 (*Continued.*)

CME date	Initial T (UT)	V (km s^{-1})	W (°)	T_O (h)	T_R (h)	T_D (h)	Source region
001124	4:21	910	71	2.1	1.5	...	N25W09
001124	15:01	1187	61	1.2	1	8	N16W19
001125[c]	1:07	2519	118	11	25.5	15	N07E50
001228	11:53	848	161	4.6	3	38.5	N19E20
2001							
010120	21:01	1330	83	5.1	3.5	9.5	N06E33
010128	15:20	766	88	3.1	1.5	16	N01W45
010211	0:20	961	123	3.1	1.5	15	N16W21
010310	3:30	819	81	7	3.5	9	N27W42
010329	9:43	797	162	2.3	4.5	29.5	N16W20
010402	10:47	859	75	1.7	1.5	...	N15W63
010402	20:56	1279	124	1.6	9	17.5	N09W55
010409	15:29	1115	116	2.6	1	...	S19W18
010410	5:17	1945	85	3.2	4.5	23	S15W14
010412	10:14	1064	114	3.7	2	12.5	S16W30
010415[c]	13:30	1199	85	0.5	2.5	11.5	S20W85
010426	12:47	1094	103	3.7	19.5	14	N15E22
010507	11:52	1053	118	0.7	3.5	21.5	N21W39
010604	15:54	623	68	1.6	0.5	10	N23W45
010711[b]	23:55	736	148	3.1	8	9	S20W65
010719	9:54	1084	86	5.1	1	21	S21W50
010809	10:09	479	87	7.3	6.5	...	N08W44
010809[b]	21:05	909	100	9.4	2.5	6	S30E90
010814	14:02	920	124	2.4	3.5	15	N30W10
010815	23:36	1504	94	1.4	1.5	22.5	S15W20
010912	21:20	668	114	6.2	1.5	21	S20W75
010915	11:10	570	75	0.3	2.5	5.5	S05W50
010924	10:15	2253	98	1.3	9.5	21	S15E26
011001[b]	5:30	1405	114	4.5	5.5	11.5	S18W80
011009	10:40	910	114	8.3	0.5	24	S26E02
011019	0:10	510	117	2.9	2	...	N19W10
011019	16:34	807	135	1.5	0.5	...	N16W20
011022	14:57	1248	100	1.1	3.5	6	S15E15
011104	16:21	1658	140	1.1	5.5	25	N08W25
011117	4:38	1115	108	3.9	20.5	34	N11E36
011122	20:39	1412	62	0.3	...	...	S09W29
011122	23:06	1566	117	2.4	5.5	24.5	N11W30
011214	8:50	1506	180	26	16.5	42	N06E90
011226	4:49	1197	106	0.7	2.5	12.5	N09W39
2002							
020315	22:32	951	104	3.5	6	23	N18W10
020318	2:25	1248	62	4.6	20	10	N03W17

Table 1 (*Continued.*)

CME date	Initial T (UT)	V (km s^{-1})	W (°)	T_O (h)	T_R (h)	T_D (h)	Source region
020411	16:01	613	43	3	3	7	S10W44
020417	8:03	1053	96	3	4	8	N16W35
020421	1:10	1894	82	0.3	5.5	26	S05W31
020522	3:36	1433	102	4	13.5	11	S15W20
020715	19:09	1033	86	14.9	9	17	N16E10
020803	18:18	971	55	3.8	1	5.5	S04W30
020814	1:52	1115	87	0.7	5.5	8.5	N11W45
020816	6:06	1176	85	1.9	0.5	6.5	N12W52
020816	12:47	1853	70	3.7	5.5	26	S10E12
020818	20:55	695	54	2	0.5	15.5	S29W11
020822	1:39	889	125	1.3	1	16	S21W50
020824[d]	1:07	1740	89	1.4	1	21	S15W31
020905	16:16	1934	54	7.8	10.5	25.5	S09E20
021109	13:12	1730	81	2.3	7	9	S12W25
021124	19:53	848	118	11.1	3	33.5	N30E10
021219	21:16	807	106	1.3	1	7.5	N16W20

Events refer to the data in Kahler (2005).

[a]Because of blurred observation images (cases 000501, 020414) and complex CME structures (cases 000510, 010324, 010615, 020220, 020520), these events are excluded from this paper. When the CME source regions are near the center of the solar disk, and the leading edges of CMEs are irregular (cases 980126, 010326, 020320) or the speed at the central part is much greater than that at the limb (case 010121), the geometrical parameters cannot be well fitted by the ice-cream cone model or approximated by its projection within the plane of the sky. These CME events are also excluded. In addition, the SEP intensity-time profile of event 980506 is more likely to be an impulsive SEP, so this event is ignored.

[b]Non-halo events with obvious asymmetry of projected morphology. These events came from the source regions near the solar limb, and their kinematic parameters are approximated by the projected values within the plane of the sky.

[c]Non-halo events with the central speed much greater than the limb speed and the source regions near the solar limb. The projected values within the plane of the sky are adopted as the CME spatial parameters.

[d]For a halo CME on 24 August 2002, the source region is identified to be S02°W81° by Kahler (2005) and S20°W37° by Michalek, Gopalswamy, and Yashiro (2007). The latter identification is used in our fitting procedure, because there is indeed transient brightening on S20°W37° from EIT images.

. . .: Data gap or overlapping of multiple events.

between the SEP onset and an occasion when the SEP intensity reaches half-peak intensity. The definition of T_R applies to the majority or nearly all of the rising phase of the SEP intensity, without the determination of occurrence of SEP peak intensity. The exact time of the peak intensity is not always explicitly known, as the second peak generally appears in the SEP intensity-time profile when the CME-driven shock arrives at 1 AU. It takes the time of $T_O + T_R$ for a SEP event to reach half of its peak intensity after the CME initiation. T_D refers to the duration over which the SEP intensity is above one half of its peak value. The time of maximum SEP intensity usually precedes the arrival time of the interplanetary shock. For some SEP cases, the time after the shock arrival is excluded from T_D.

The rise time T_R and the duration T_D are the same as the values in Kahler (2005), while the onset time T_O is different in this paper. The difference in T_O is due to the estimation of the CME initiation time, because the radial speeds of CMEs inferred from the ice-cream cone

model are different from the projected speed derived in Kahler (2005). The overlapping of intensity-time profiles of two SEP events or a gap in observation data has led to uncertainty of T_R in one event and of T_D in eight events. The values of T_O, T_R, and T_D of SEP events in this paper are summarized in columns 5 – 7 of Table 1.

2.4. Correlation Analyses

The longitude of CME source regions has a great effect on the scatter in SEP characteristic times, as shown in Figure 1. There is a trend of diminishing SEP characteristic times as the longitude of CME source regions is shifted from east to west. The average and dispersion in T_O are relatively small in the west, whereas those of T_R and T_D reach the minimum within W30° – W60°, which is consistent with previous statistical results (Cane, Reames, and von Rosenvinge, 1988; Balch, 1999). The distributions of CME speed and width on the heliographic longitude are also given in Figure 1, and they are independent of the heliographic longitude.

The magnetic field lines connected to the Earth are rooted at about W60° on the solar surface (Shen *et al.*, 2006), if the solar wind travels at a speed of about 400 km s^{-1}. For CMEs originating from the east and 0° – W29° of the solar disk, the nose of the CME-driven shock would be far away from the Earth in terms of magnetic connection. The accelerated particles at the shock front would transversely diffuse across the IMF lines before its arrival at the Earth. The longer time required for the solar wind to convect field lines past the Earth allows for more cross-field scattering of the particles, hence longer SEP time scales. The SEP characteristic times may be affected by the local plasma properties in the interplanetary region along the transverse SEP trajectory, leading to large scatter in the SEP time scales. For a gradual SEP event, its associated CME event usually has large angular width (Kahler, 2004). If a CME occurs within longitudes W30° – W90°, its solar source region is magnetically well connected to the Earth across the nose of the CME-driven shock, and the shock mode at the acceleration site of the SEP event is mainly quasi-parallel. Therefore, for the occurrence of CMEs within W30° – W90°, the acceleration site is magnetically well connected to the Earth by one bundle of IMF lines, the accelerated particles would be guided by these IMF lines to reach the Earth, and the ensuing SEP events will have a relatively simple acceleration mechanism and transport process. For these specific SEP events, it is more favorable to find the statistical correlation between the geometric parameters of CMEs and the characteristic times of SEP events observed at 1 AU.

In this paper, the source regions of CME initiation are classified into four groups in terms of magnetic connection in longitude. The regions of E90° – E1° (22 events) and 0° – W29° (28 events) are far away from the Earth in terms of magnetic connection (poorly connected), and those of W30° – W59° (30 events) and W60° – W90° (15 events) are close to the Earth in magnetic linkage (magnetically well connected). For each longitudinal region, we have studied the correlation between the characteristic times of SEP events and the radial speed (V) and angular width (W) of the associated CME events. The correlation coefficients (R) and rejection probabilities of correlation (P) are summarized in Table 2. A significant correlation may be claimed if $P \leq 0.02$.

2.4.1. Correlation Between Characteristic Times of SEP and Radial Speed of CME

There is no significant correlation between the SEP onset time T_O and the CME radial speed V for all longitudinal regions. For the poorly connected regions (E90° – E1° and W0° – W29°), the CME source regions are far away from the Earth in terms of magnetic connection, and the SEP rise time T_R and duration T_D are not significantly correlated with the CME radial speed V.

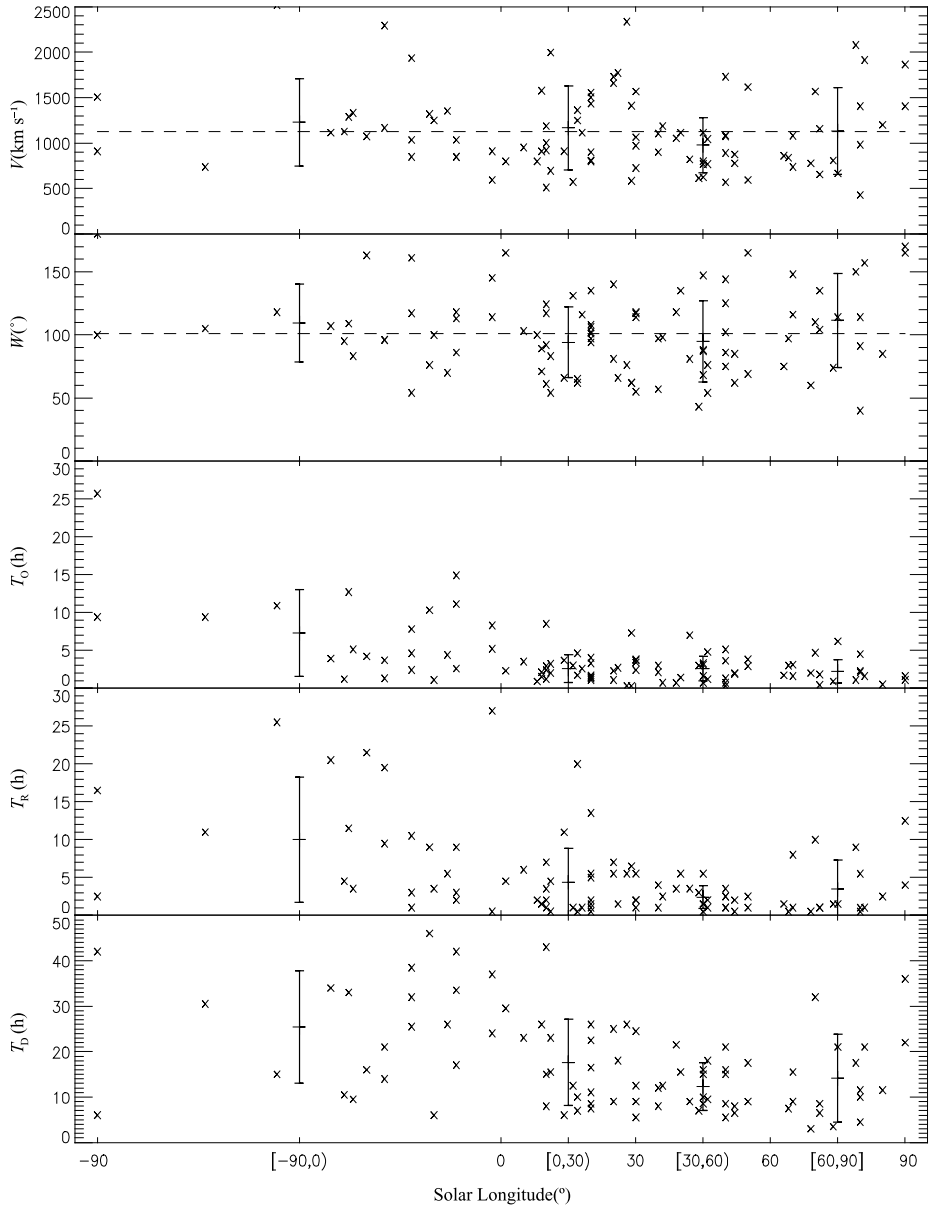

Figure 1 Geometrical parameters of CMEs and characteristic times of the associated SEP events as a function of the heliographic longitude of the CME source location. From top to bottom are the CME speed V, angular width W, SEP onset time T_O, SEP rise time T_R, and SEP duration T_D. The standard deviations of longitudinal bins indicated on the abscissa are shown as error bars. The average speed of 1103 km s^{-1} and average width of 102° are denoted by the dashed lines.

The scatter plots of T_R versus V and their linear regression analysis are given in the left column of Figure 2 for events magnetically well connected to the Earth. The T_R–V correlation for the regions of W30° – W59° is insignificant with correlation coefficient $R =$

Table 2 Correlation coefficient and probability between SEP characteristic times and CME radial speed[a].

CME parameter	R/P with T_O	R/P with T_R	R/P with T_D
All events (95)[b]			
V	0.06/0.56	0.32/< 0.01	0.23/0.03
W	0.16/0.11	0.24/0.02	0.40/< 0.01
[E90°, E1°][c] (22)			
V	0.08/0.71	0.23/0.30	−0.22/0.32
W	0.28/0.20	0.33/0.14	0.31/0.16
[W0°, W29°] (28)			
V	−0.19/0.33	0.22/0.27	0.07/0.76
W	−0.01/0.97	−0.23/0.24	0.39/0.08
[E90°, W29°] (50)			
V	0.10/0.51	0.27/0.06	−0.07/0.65
W	0.24/0.10	0.16/0.28	0.38/0.01
[W30°, W59°] (30)			
V	−0.31/0.10	0.34/0.07	0.66/< 0.01
W	−0.07/0.70	0.35/0.06	0.43/0.02
[W60°, W90°] (15)			
V	−0.15/0.59	0.65/0.01	0.73/< 0.01
W	−0.02/0.94	0.66/0.01	0.60/0.02
[W30°, W90°] (45)			
V	−0.25/0.10	0.46/< 0.01	0.69/< 0.01
W	−0.07/0.66	0.47/< 0.01	0.46/< 0.01

[a]Columns from left to right are geometrical parameters and their correlation coefficient R and rejection probability P with respect to the SEP characteristic times T_O, T_R, and T_D, respectively.

[b]Number of events in the longitude range.

[c]Range of heliographic longitudes of the source region of the associated CME.

0.34 and rejection probability $P = 0.07$. In contrast, for the regions of W60° – W90°, T_R and V exhibit significant positive correlation with $R = 0.65$ and $P = 0.01$. Specifically, every 100 km s^{-1} increase in V leads to a corresponding increase of 0.6 hour for T_R. In addition, significant positive correlation between T_R and V appears for regions between W30° and W90°, with $R = 0.46$, $P < 0.01$, and T_R increases by 0.3 hour for every increase of 100 km s^{-1} in V. Hence, we may conclude that significant positive correlation between T_R and V exists for SEP events in well-connected regions.

The right column of Figure 2 shows the scatter plots of SEP duration T_D versus V and their linear regression analysis for events magnetically well connected to the Earth. For the regions of W30° – W59° (W60° – W90°), the T_D–V correlations are significantly positive with $R = 0.66$ (0.73), $P < 0.01$, and T_D increases by 1.2 (1.7) hours for an increase of every 100 km s^{-1} in V, respectively. Significant positive correlation between T_D and V also holds for the regions of W30° – W90°, with $R = 0.69$, $P < 0.01$, and T_D increases by 1.4 hours for an increase of every 100 km s^{-1} in V. Moreover, the T_D–V correlation is better than the T_R–V correlation. Therefore, from our statistical studies, for SEP events magnetically

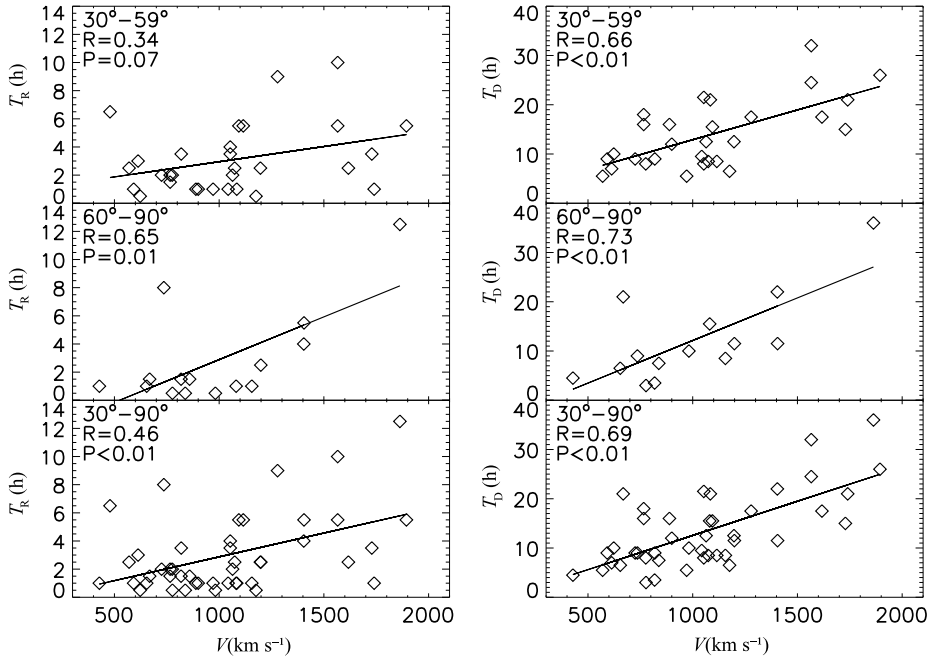

Figure 2 The scatter plots of SEP characteristic times T_R (left) and T_D (right) in terms of the associated CME speed V for the well-connected events. The longitude ranges of the CME source locations are [W30°, W59°], [W60°, W90°], and [W30°, W90°], from top to bottom, respectively. The linear regression is shown in each panel with the value of correlation coefficient R and rejection probability of correlation at the upper left corner. The correlation is significant for $P \leq 0.02$.

well connected to the Earth, both T_R and T_D are significantly correlated with V in a positive manner.

Kahler (2005) found that *i*) for CME source regions in W65° – W90°, T_R and T_D are significantly correlated with the projected CME speed within the plane of the sky, and *ii*) the correlation coefficients are 0.48 and 0.53, respectively, which is confirmed by our statistical studies in this paper as well. However, in Kahler's (2005) study, no significant correlation between T_D and the projected CME speed is found for the regions of W32° – W62°. This discrepancy between our study and Kahler's may be ascribed to our usage of the CME ice-cream cone model and the use of CME projected speed by Kahler. The true speed of CMEs is better approximated by the ice-cream cone model. When a CME source region is near the solar limb (*i.e.*, W65° – W90°), both the projected speed and the speed from the cone model are close to the true speed; when a source region is farther away from the solar limb (*i.e.*, W32° – W62°), the above two speeds differ greatly.

2.4.2. Correlation Between Characteristic Times of SEP and Angular Width of CME

There is no significant correlation between T_O and W in our statistical studies in every longitudinal region. For SEP events in the poorly connected regions, T_R is not significantly correlated with W. T_D and W exhibit a positive correlation with $R = 0.38$, $P = 0.01$ in regions E90° – W29°, but there are no significant correlations between T_D and W for the SEP event groups of E90° – E1° and W0° – W29° separately. Thus, we consider that the

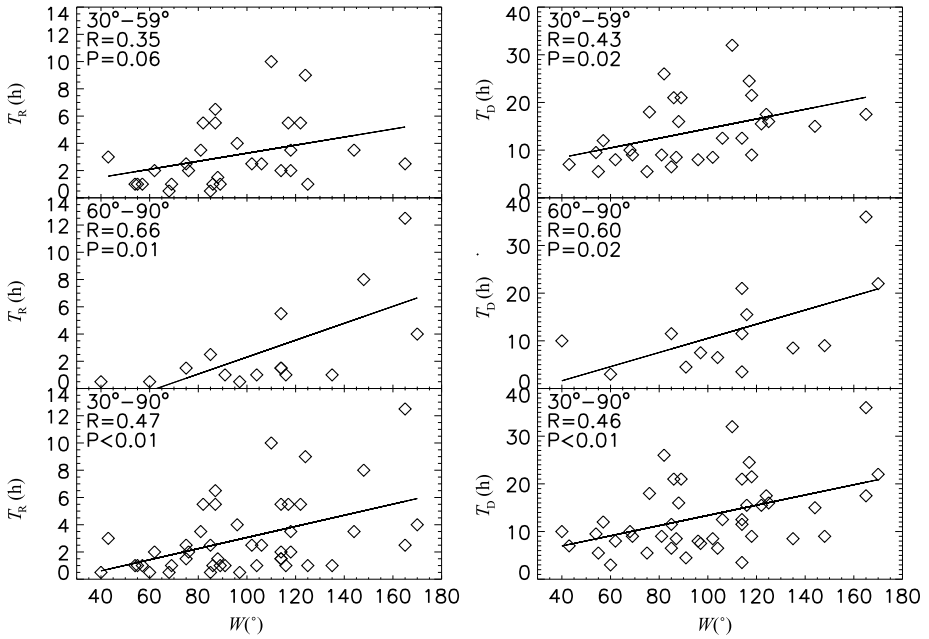

Figure 3 The same as Figure 2, but in terms of the CME width W.

SEP rise time T_R is not significantly correlated with the CME angular width W for the SEP events in the poorly connected regions, while the SEP duration T_D may be weakly correlated with W.

The scatter plots of SEP rise time T_R versus W and their linear regression analysis are shown in the left column of Figure 3 for well-connected events. The $T_R - W$ correlation for the region of W30° – W59° is insignificant with correlation coefficient $R = 0.35$ and rejection probability $P = 0.06$. As a comparison, for regions of W60° – W90°, T_R and W exhibit significant positive correlation with $R = 0.66$, $P = 0.01$, and T_R increases by 0.6 hour for an increase of every 10° in W. For regions of W30° – W90°, T_R and W are also correlated with $R = 0.47$, $P < 0.01$, and T_R increases by 0.4 hour for an increase of every 10° in W. Hence, significant positive correlation between T_R and W exists for SEP events that are magnetically well connected to the Earth.

The scatter plots of SEP duration T_D versus W and their linear regression analysis are shown in the right column of Figure 3. For the regions of W30° – W59° (W60° – W90°), the T_D–W correlations are significantly positive with $R = 0.43$ (0.60), $P = 0.02$, and T_D increases by 1.0 (1.5) hours for an increase of every 10° in W, respectively. Similarly, for the regions of W30° – W90°, T_D and W are also significantly correlated with $R = 0.46$, $P < 0.01$, and T_D increases by 1.1 hours for an increase of every 10° in W. Therefore, according to our statistical studies, the correlations of T_R versus W and T_D versus W are significant and positive for the magnetically well-connected longitudes.

Kahler (2005) found that both T_R and T_D are weakly correlated with the projected width of CMEs for events magnetically well connected to the Earth. His correlation analysis is suggestive but not definitive, because the significance of the correlation may be masked by a large number of halo CMEs. Otherwise, we would have obtained much more enhanced positive correlations for both T_R and T_D versus W, since the true angular width of a CME

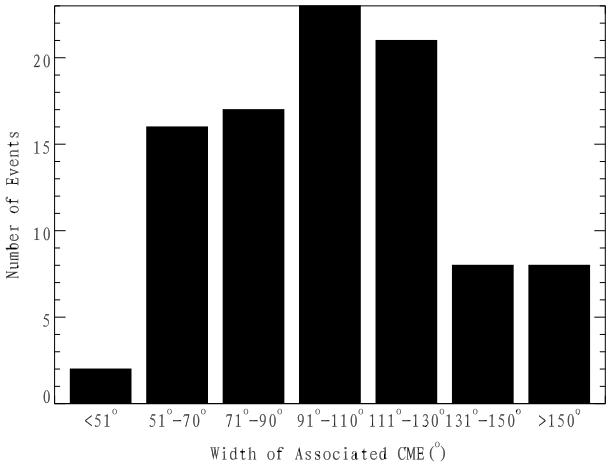

Figure 4 Number of SEP events in terms of the width of the associated CMEs.

is better approximated by the ice-cream cone model in this paper. The distribution of SEP events with the CME angular width is given as a histogram plot in Figure 4. The average angular width of all CMEs in Figure 4 is 102°.

3. Summary and Discussion

Whether and how the intensity of SEP events depends on the formation and dynamics of coronal/interplanetary shocks driven by CMEs are still not well understood. In this paper, the ice-cream cone model is applied to calculate the realistic kinematic parameters of CMEs, namely, the radial speed, angular width, and heliographic location of the solar source region. Then these CME kinematic parameters are statistically analyzed for possible correlation with the characteristic times of the intensity-time profile of associated gradual SEP events observed at 1 AU.

For any longitude of CME initiation at the solar surface, both the radial speed and angular width of a CME are not significantly correlated with the onset time T_O of the associated SEP. T_O is the time contributed from the following processes: *i*) the formation time of the CME-driven shock just after the main acceleration phase of a CME, *ii*) the trapping, accelerating, and escaping times of energetic particles at the CME-driven shock front, and *iii*) the transport time of the accelerated particles in the Sun–Earth space. It is difficult to expect significant relations between T_O and CME geometric parameters. For CMEs with solar source regions that are far away from the Earth in terms of magnetic connection, there is no significant correlation between the characteristic times of SEP events and kinematic parameters of CMEs. In these cases, the SEP characteristic times are more likely to be affected by diffusion processes other than CME kinematic parameters. The diffusion of charged particles in directions perpendicular to the large-scale average magnetic field is intrinsically nonlinear and is caused by turbulence, which has substantial transverse structure. Therefore, such a process will result in energetic particles moving along complicated routes (Qin, Matthaeus, and Bieber, 2002; Qin and Li, 2008).

Our statistical results show that, for SEP events magnetically well connected to the Earth, the radial speed of CMEs shows significantly positive correlation with respect to both the

rise time T_R and the duration T_D of the associated SEP events. This indicates that energetic particles could be entrapped and accelerated for a longer time for fast CMEs, since a faster CME can continuously drive a stronger coronal/interplanetary shock. As a result, both T_R and T_D would be larger. This is consistent with the statistical studies of Kahler (2005), but with better correlations. Meanwhile, both the rise time T_R and duration T_D of SEP events also show significantly positive correlation with respect to the angular width of the associated CMEs. The shock driven by a wider CME corresponds to longer T_R and T_D. During the anti-Sunward propagation of an interplanetary shock, the Earth-connected magnetic field lines along the shock front are gradually shifted from west to east. For a wider shock front driven by a wider CME, those energetic particles, connected to the Earth by the IMF, can stay for a longer time within the shock nose, and the shock mode at the acceleration site of the SEP event is quasi-parallel. Then the trapping and acceleration of energetic particles last for a longer time, increasing T_R and T_D accordingly. A similar scenario was proposed by Kahler (2005). However, he used the projected angular width of CMEs in the plane of the sky, which can be quite different from the true angular width in three dimensions. As a result, only weak correlation was present in the statistical studies of Kahler (2005).

In summary, a faster and wider CME could drive a stronger and wider shock, which can entrap and accelerate particles for a longer time, resulting in longer rise time and duration of SEP events. When the shock is stronger, some of the particles in the upstream of the shock front are more easily accelerated to a higher energy. These energized particles will excite various plasma waves with a wide spectrum of frequencies, producing strong plasma turbulence along the shock front. The feedback of turbulence generation is further favorable for the shock to entrap energetic particles. Being entrapped in a high energy potential across the shock front, these particles are continuously accelerated back and forth, crossing the shock front. Only sufficiently energized particles can escape from the shock front. As a result, the rise time T_R and duration T_D of the SEP events are significantly prolonged for a strong and wide shock.

Acknowledgements ZHP and CBW were supported by the National Nature Science Foundation (40774076, 40931053, 40874075) and the Chinese Academy of Sciences (KZCX2-YW-QN512). YW was supported by the National 973 key project (2011CB811403). XHX was supported by the Specialized Research Fund for the Doctoral Program of Higher Education (200803581019). We are grateful for the use of observational data from the SOHO and *Yohkoh* spacecraft in this paper. The reference of the LASCO CME catalog is also acknowledged. This CME catalog is generated and maintained by the Center for Solar Physics and Space Weather, the Catholic University of America, in cooperation with the Naval Research Laboratory and NASA.

References

Balch, C.C.: 1999, *Radiat. Meas.* **30**, 231.
Cane, H.V., Reames, D.V., von Rosenvinge, T.T.: 1988, *J. Geophys. Res.* **93**, 9555.
Cliver, E.W., Kahler, S.W., Reames, D.V.: 2004, *Astrophys. J.* **605**, 902.
Dai, Y., Tang, Y.H., Qiu, K.P.: 2005, *Adv. Space Res.* **35**, 1871.
Decker, R.B., Vlahos, L.: 1986, *Astrophys. J.* **306**, 710.
Fisher, R.R., Munro, R.H.: 1984, *Astrophys. J.* **280**, 428.
Giacalone, J.: 2005a, *Astrophys. J.* **624**, 765.
Giacalone, J.: 2005b, *Astrophys. J. Lett.* **628**, 37.
Gopalswamy, N., Yashiro, S., Kaiser, M.L., Howard, R.A., Bougeret, J.-L.: 2001, *J. Geophys. Res.* **106**, 29219.
Gopalswamy, N., Lara, A., Manoharan, P.K., Howard, R.A.: 2005a, *Adv. Space Res.* **36**, 2289.
Gopalswamy, N., Yashiro, S., Liu, Y., Michalek, G., Vourlidas, A., Kaiser, M.L., Howard, R.A.: 2005b, *J. Geophys. Res.* **110**, A09S15.
Howard, R.A., Michels, D.J., Sheeley, N.R., Koomen, M.J.: 1982, *Astrophys. J.* **263**, 101.

Jokipii, J.R.: 1982, *Astrophys. J.* **255**, 716.
Jokipii, J.R.: 1987, *Astrophys. J.* **313**, 842.
Kahler, S.W.: 2001, *J. Geophys. Res.* **106**, 20947.
Kahler, S.W.: 2004, *Astrophys. J.* **603**, 330.
Kahler, S.W.: 2005, *Astrophys. J.* **628**, 1014.
Kahler, S.W., Reames, D.V.: 2003, *Astrophys. J.* **284**, 1063.
Kahler, S.W., Vourlidas, A.: 2005, *J. Geophys. Res.* **110**, A12S01.
Kahler, S.W., McAllister, A.H., Cane, H.V.: 2000, *Astrophys. J.* **533**, 1063.
Kallenrode, M.-B.: 2003, *J. Phys. G, Nucl. Part. Phys.* **29**, 965.
Kocharov, L., Torsti, J., Laitinen, T., Teittinen, M.: 1999, *Solar Phys.* **190**, 295.
Leblanc, Y., Dulk, G.A., Vourlidas, A., Bougeret, J.-L.: 2001, *J. Geophys. Res.* **106**, 25, 301.
Michalek, G., Gopalswamy, N.: 2003, *Astrophys. J.* **584**, 472.
Michalek, G., Gopalswamy, N., Yashiro, S.: 2007, *Solar Phys.* **246**, 399.
Michalek, G., Gopalswamy, N., Lara, A., Manoharan, P.K.: 2004, *Astron. Astrophys.* **423**, 729.
Ostrowski, M.: 1991, *Mon. Not. Roy. Astron. Soc.* **249**, 551.
Qin, G., Li, G.: 2008, *Astrophys. J.* **682**, 129.
Qin, G., Matthaeus, W.H., Bieber, J.W.: 2002, *Astrophys. J.* **578**, 117.
Reames, D.V.: 1999, *Space Sci. Rev.* **90**, 413.
Reames, D.V., Kahler, S.W., Ng, C.K.: 1997, *Astrophys. J.* **491**, 414.
Shen, C.L., Wang, Y.M., Ye, P.Z., *et al.*: 2006, *Astrophys. J.* **639**, 510.
Tang, Y.H., Dai, Y.: 2003, *Adv. Space Res.* **32**, 2609.
Torsti, J., Kocharov, L., Innes, D.E., Laivola, J., Sahla, T.: 2001, *Astron. Astrophys.* **365**, 198.
Tylka, A.J.: 2001, *J. Geophys. Res.* **106**, 25333.
Tylka, A.J., Lee, M.A.: 2006, *Astrophys. J.* **646**, 1319.
Tylka, A.J., Cohen, C.M.S., Dietrich, W.F., Lee, M.A., Maclennan, C.G., Mewaldt, R.A., Ng, C.K., Reames, D.V.: 2005, *Astrophys. J.* **625**, 474.
Wang, Y.M., Shen, C.L., Wang, S., Ye, P.Z.: 2004, *Solar Phys.* **222**, 329.
Wang, Y.M., Xue, X.H., Shen, C.L., Ye, P.Z., Wang, S., Zhang, J.: 2006, *Astrophys. J.* **646**, 625.
Webb, G.M., Zank, G.P., Ko, C.M., Donohue, D.J.: 1995, *Astrophys. J.* **453**, 178.
Xie, H., Ofman, L., Lawrence, G.: 2004, *J. Geophys. Res.* **109**, A03109.
Xie, H., Gopalswamy, N., Ofman, L., St. Cyr, O.C., Michalek, G., Lara, A., Yashiro, S.: 2006, *Space Weather* **4**, S10002.
Xue, X.H., Wang, C.B., Dou, X.K.: 2005, *J. Geophys. Res.* **110**, A08103.
Zhao, X.P., Plunkett, S.P., Liu, W.: 2002, *J. Geophys. Res.* **107**(A8), SSH13-1.